Available online at www.sciencedirect.com
SCIENCE DIRECT®
Journal of Computational Physics 206 (2005) 81–94
JOURNAL OF COMPUTATIONAL PHYSICS
www.elsevier.com/locate/jcp

Distributed Lagrange multiplier/fictitious domain method in the framework of lattice Boltzmann method for fluid–structure interactions

Xing Shi *, Nhan Phan-Thien

Division of Bioengineering, National University of Singapore, 10 Kent Ridge Crescent, Singapore 119260, Singapore

Received 22 March 2004; received in revised form 2 November 2004; accepted 7 December 2004
Available online 9 February 2005

Abstract

A new implementation of the lattice Boltzmann method (LBM) for fluid–structure interactions is presented. The idea of the distributed-Lagrange-multiplier/fictitious-domain method (DLM/FD) is introduced in the framework of the lattice Boltzmann algorithm. This implementation employs a fixed mesh for the solution of the fluid problem and a Lagrangian formulation for the solid problem. The main advantage of the method is that the re-meshing procedure normally required in the ALE method is circumvented. Numerical examples are provided to verify the algorithm and illustrate the capacity of the method to deal with the fluid/elastic–solid interactions.

Keywords: Fluid–structure interactions; Lattice Boltzmann method; Fictitious domain method; Distributed Lagrange multiplier

1. Introduction

Although the lattice Boltzmann method has been widely used in different areas of computational fluid dynamics (CFD) [1,2], such as hydrodynamics, complex fluids, suspensions, turbulent flows, microfluidics [3] and visco-elastic fluids [4,5], its applications in fluid–structure interaction problems [6,7] are still very limited. Fluid–structure interactions include fluid/rigid–solid interactions and fluid/elastic–solid interactions, and in both cases, how to cope with the moving fluid–solid interface is a critical problem.

* Corresponding author.
E-mail addresses: biesx@nus.edu.sg, mecshix@yahoo.com (X. Shi).

0021-9991/$ - see front matter
doi:10.1016/j.jcp.2004.12.017

In the lattice Boltzmann method, a popular scheme for the fluid–structure interactions including the particulate flows [8,9] is based on the bounce-back rule enforcing the no-slip condition on the solid surface. Such a scheme is suitable for the rigid-solid case where the motion of the solid is determined only by the total force and torque exerted on the body. However, for the elastic-body case where the motion of the solid is determined by the local stress state, a very fine mesh might be required for high accuracy. Recently, Feng and Michaelides [10] combined the immersed boundary method [11] and the lattice Boltzmann method to simulate the particulate flows, and provided an alternative approach to handle the moving fluid–solid boundary in the lattice Boltzmann method.

There exist a variety of methods for the fluid–structure interactions where the flow is solved from the Navier–Stokes equation rather than the lattice Boltzmann equation. These methods can be classified into two categories, depending on whether the moving mesh or the fixed-mesh is used to solve the Navier–Stokes equation. For the methods based on the moving mesh technique, such as the arbitrary Lagrangian–Eulerian method (ALE) [12], the boundary-fitted mesh is updated with the structure motion, hence the boundaries are described accurately. But the trade-off is the high computational cost due to the re-meshing procedure. When the boundaries are complex such as concentrated particulate flows, re-meshing is very difficult, if not impossible. For the fixed-mesh-based methods, the fluid mesh is not altered by the solid motion, and re-meshing is not required, therefore such methods are simpler and more efficient than the moving-mesh-based methods. The distributed-Lagrange-multiplier/fictitious-domain method (DLM/FD) is a popular fixed-mesh-based method, and has been applied to the Dirichlet problem [13], external incompressible viscous flows [14], fluid-rigid particle systems [15] and viscoelastic mobility problems [16]. Recently, Baaijens and co-workers [17,18] extended the DLM/FD method to the fluid/elastic–body interactions, and Yu [19] derived a more general formation. The basic idea of the DLM/FD method is that the fluid region is extended to the solid region and a distributed Lagrange multiplier is introduced to enforce the fictitious fluids in the solid region to satisfy the constraint of the solid motion. The distributed Lagrange multiplier can be physically interpreted as a pseudo body force, allowing the combination of the DLM/FD method and the LBM.

The purpose of this paper is to extend the LBM to fluid–structure interaction problems by using the idea and technique of the DLM/FD method. The paper is organized as follows: Section 2 describes the governing equations and the proposed LBM-DLM/FD method. The benchmark problem of the flow past a circular cylinder is utilized to verify the method for the case of rigid-body in Section 3.1, and the power of the method will be illustrated by the solution of an elastic beam flapping in a cylinder weak in Section 3.2.

2. Governing equations

2.1. Fluid domain

The fluid flow is solved by the lattice Boltzmann method. Unlike the continuum fluid equations, the lattice Boltmznn equations are derived from a microscopic kinetics theory. The discrete lattice Boltzmann equations of a single relaxation time model under external forces are reproduced here [2,20]:

$$f_i(t+\delta_t, \mathbf{x}+\mathbf{e}_i\delta_t) = f_i(t,\mathbf{x}) - \frac{1}{\tau}(f_i - f_i^{\mathrm{eq}}) + \frac{\mathbf{F}\cdot(\mathbf{e}_i-\mathbf{u}_\mathrm{f})}{\rho_\mathrm{f} c_\mathrm{s}^2} f_i^{\mathrm{eq}}\delta_t, \tag{1}$$

where $f_i(t,\mathbf{x})$ is the single-particle distribution function on the i-direction microscopic velocity $\mathbf{e}_i$, $\mathbf{F}$ is the external force, τ is the relaxation time that is related to the kinematic viscosity of fluids, δ_t denotes the time step, $\Omega_i = -\frac{1}{\tau}(f_i - f_i^{\mathrm{eq}})$ designates the collision operator, and $\mathbf{u}_\mathrm{f}$, ρ_f are the macroscopic velocity and mass density of the fluid, respectively, which can be obtained from the distribution functions as follows [1]:

$$\rho_\mathrm{f} = \sum_i f_i, \quad \rho_\mathrm{f}\mathbf{u}_\mathrm{f} = \sum_i f_i \mathbf{e}_i. \tag{2}$$

For the so-called 2D 9-bit BGK model [21] used here, the discrete velocities are

$$\begin{aligned}\mathbf{e}_0 &= (0,0),\\ \mathbf{e}_i &= \left(\cos\left(\frac{(i-1)}{4}\pi\right), \sin\left(\frac{(i-1)}{4}\pi\right)\right)\frac{\delta_x}{\delta_t}, \quad i = 1,\ldots,8,\end{aligned} \tag{3}$$

where δ_x is the lattice spacing. The corresponding equilibrium distribution functions can be chosen in the following form [21]:

$$f_i^{\mathrm{eq}} = w_i\rho_{\mathrm{f}}\left[1 + \frac{3}{c^2}(\mathbf{e}_i\cdot\mathbf{u}_{\mathrm{f}}) + \frac{9}{2c^4}(\mathbf{e}_i\cdot\mathbf{u}_{\mathrm{f}})^2 - \frac{3}{2c^2}\mathbf{u}_{\mathrm{f}}^2\right], \tag{4}$$

where $c = \delta_x/\delta_t$ ($c_{\mathrm{s}} = c/\sqrt{3}$ is the sound speed), and w_i is the weight with the following values:

$$\begin{aligned}w_0 &= \frac{4}{9},\\ w_i &= \frac{1}{9}, \quad i = 1,3,5,7,\\ w_i &= \frac{1}{36}, \quad i = 2,4,6,8.\end{aligned} \tag{5}$$

With the help of the Chapman–Enskog procedure, the macroscopic mass and momentum equations can be recovered [1,21]:

$$\frac{\partial\rho_{\mathrm{f}}}{\partial t} + \nabla\cdot(\rho_{\mathrm{f}}\mathbf{u}_{\mathrm{f}}) = 0, \tag{6}$$

$$\frac{\partial(\rho_{\mathrm{f}}\mathbf{u}_{\mathrm{f}})}{\partial t} + \nabla\cdot(\rho_{\mathrm{f}}\mathbf{u}_{\mathrm{f}}\mathbf{u}_{\mathrm{f}}) = \nabla\cdot\left(-c_{\mathrm{s}}^2\rho_{\mathrm{f}}\mathbf{I} + \rho_{\mathrm{f}}\nu(\nabla\mathbf{u}_{\mathrm{f}} + \nabla\mathbf{u}_{\mathrm{f}}^{\mathrm{T}})\right) + \mathbf{F}. \tag{7}$$

In the D2Q9 model, the kinematic viscosity is $\nu = \frac{1}{6}(2\tau - 1)\frac{\delta_x^2}{\delta_t}$. For a nearly incompressible fluid, we require $|\mathbf{u}_{\mathrm{f}}| \ll |\mathbf{e}_i|$ and the evolution equation (1) is simplified to:

$$f_i(t+\delta_t, \mathbf{x} + \mathbf{e}_i\delta_t) = f_i(t,\mathbf{x}) - \frac{1}{\tau}(f_i - f_i^{\mathrm{eq}}) + \frac{w_i\delta_t}{c_{\mathrm{s}}^2}(\mathbf{F}\cdot\mathbf{e}_i). \tag{8}$$

2.2. Solid domain

In the current study, we neglect the inertia and gravity terms, thus the solid momentum equation reduces to

$$\nabla\cdot\boldsymbol{\sigma}_{\mathrm{s}} = 0, \tag{9}$$

where $\boldsymbol{\sigma}_{\mathrm{s}}$ is the Cauchy–Green stress tensor. In this paper, we assume that the solid material satisfies the neo-Hookean constitutive law with the strain energy density [22]:

$$W = C_1\left(I_1 I_3^{-\frac{1}{3}} - 3\right) + \frac{K}{2}(J-1)^2, \tag{10}$$

where C_1 is the shear modulus and K is the bulk modulus to model the material compressibility. I_1 and I_3 are the first and the third invariants of the Green's deformation tenor respectively. $J = \det(\mathbf{F}_{\mathrm{d}})$, $\mathbf{F}_{\mathrm{d}}$ is the deformation gradient tension defined by:

$$\mathbf{F}_{\mathrm{d}} = \frac{\partial\mathbf{x}}{\partial\mathbf{X}_0},$$

where $\mathbf{X}_0$ denotes the reference configuration and $\mathbf{x}$ denotes the current configuration. The left Cauchy–Green tensor is defined as $\mathbf{B} = \mathbf{F}_{\mathrm{d}}\mathbf{F}_{\mathrm{d}}^{\mathrm{T}}$, and the Cauchy–Green stress can be written as:

$$(\sigma_s)_{ij} = 2C_1 J^{-\frac{5}{3}}\left(B_{ij} - \frac{1}{3}B_{kk}\delta_{ij}\right) + K(J-1)\delta_{ij}. \tag{11}$$

The incompressibility of the solid material is approximated by taking a large K value.

2.3. LBM-DLM/FD method

The basic idea of the fictitious domain method is to extend a problem on a geometrically complex domain to a larger simpler domain (fictitious domain) [15]. The distributed Lagrange multiplier (DLM) is introduced to enforce the velocity constraints on the solid surface and in the solid domain. From the minimization of the energy principle, Baaijens first derived the DLM/FD formulation for a fluid/elastic–solid system as follows [17]:

The solid equation:

$$\int_{\Omega_s} (\nabla \boldsymbol{\varphi}_s) : \boldsymbol{\sigma}_s \, d\Omega_s + \int_{\Gamma} \boldsymbol{\lambda} \cdot \boldsymbol{\varphi}_s \, d\Gamma = 0. \tag{12}$$

The fluid equations,

$$\int_{\Omega_f} \rho_f \left(\frac{\partial \mathbf{u}_f}{\partial t} + \mathbf{u}_f \cdot \nabla \mathbf{u}_f\right) \cdot \boldsymbol{\varphi}_f \, d\Omega_f + \int_{\Omega_f} \left(-p\mathbf{I} + \eta\left(\nabla \mathbf{u}_f + (\nabla \mathbf{u}_f)^T\right)\right) : \nabla \boldsymbol{\varphi}_f \, d\Omega_f - \int_{\Gamma} \boldsymbol{\lambda} \cdot \boldsymbol{\varphi}_f \, d\Gamma = 0, \tag{13}$$

$$\int_{\Omega_f} (\nabla \cdot \mathbf{u}_f) q \, d\Omega_f = 0 \tag{14}$$

and the velocity constraint equation

$$\int_{\Gamma} (\mathbf{u}_s - \mathbf{u}_f) \cdot \boldsymbol{\gamma} \, d\Gamma = 0. \tag{15}$$

In above equations, p is the pressure, η is the fluid dynamic viscosity, $\boldsymbol{\varphi}_f$, q, $\boldsymbol{\varphi}_s$ and $\boldsymbol{\gamma}$ are the variances of the fluid velocity, the fluid pressure, the solid velocity or displacement and the Lagrange multiplier $\boldsymbol{\lambda}$, respectively. In the fictitious domain method, the fluid domain Ω_f includes the real fluid domain and the fictitious fluid domain (i.e., the solid domain Ω_s). The feature of the Baaijens' formulation is that the Lagrange multiplier is defined on the fluid–solid interface Γ to enforce the no-slip velocity constraint there. A more general DLM/FD formulation has been proposed by Yu recently, where the Lagrange multiplier is distributed over the solid domain Ω_s [19] and the effects of the inertia and body force terms are considered:

$$\int_{\Omega_s} \left[(\rho_s - \rho_f)\frac{d\mathbf{u}_s}{dt} - (\rho_s \mathbf{f}_s - \rho_f \mathbf{f}_f)\right] \cdot \boldsymbol{\varphi}_s \, d\Omega_s + \int_{\Omega_s} (\boldsymbol{\sigma}_s - \boldsymbol{\sigma}_f) : \nabla \boldsymbol{\varphi}_s \, d\Omega_s + \int_{\Omega_s} \boldsymbol{\lambda} \cdot \boldsymbol{\varphi}_s \, d\Omega_s = 0, \tag{16}$$

here $\mathbf{f}_f$ and $\mathbf{f}_s$ denote the fluid and solid body-forces, respectively. If we neglect the inertia and body force terms, Eq. (16) reduces to:

$$\int_{\Omega_s} (\boldsymbol{\sigma}_s - \boldsymbol{\sigma}_f) : \nabla \boldsymbol{\varphi}_s \, d\Omega_s + \int_{\Omega_s} \boldsymbol{\lambda} \cdot \boldsymbol{\varphi}_s \, d\Omega_s = 0. \tag{17}$$

If the fluid stress term is negligible compared to the solid stress term in Ω_s (as observed in [19]), Eq. (17) further reduces to

$$\int_{\Omega_s} \boldsymbol{\sigma}_s : \nabla \boldsymbol{\varphi}_s \, d\Omega_s + \int_{\Omega_s} \boldsymbol{\lambda} \cdot \boldsymbol{\varphi}_s \, d\Omega_s = 0, \tag{18}$$

which is almost the same as Eq. (12), and the only difference lies in the integral domain of the Lagrange multiplier.

In the solid and fluid equations, if the Lagrange multiplier $\boldsymbol{\lambda}$ is replaced with an external force $\mathbf{F}$, we can substitute Eq. (1) or Eq. (8) for Eqs. (13) and (14) to solve the fluid flow. This is the idea of our LBM-DLM/FD method.

The solid equation is solved by the Galerkin finite element method. In the finite element method, the solution on each element is expressed as follows:

$$a_h = \sum_{i=1}^{n} a_i N_i.$$

Here a_i are unknown constants, and N_i are linearly independent basis functions spanning on a n-dimension subspace. More details on the finite element method can be found in [23]. Nine-node biquadratic elements are employed for the solid displacement field in the current study. As required by the numerical stability, the order of the interpolation function of the Lagrange multiplier should be at least one order lower than that of the displacement [18]. Here, the Lagrange multiplier is considered as piecewise constant on each element.

As a bridge between the fluid and solid equations, the Lagrange multiplier $\boldsymbol{\lambda}$ should be known on both fluid and solid meshes. The solid mesh is different from the fluid mesh, which generates a problem in the implementation: how to project the information from the solid mesh to the fluid mesh. It is easy to get information at any location on the solid element in the finite element method, but the procedure of locating the fluid grid in the solid mesh is non-trivial. For simplicity, here we adopt the allocation functions in the immersed boundary method [24]: we first concentrate the Lagrange multiplier $\boldsymbol{\lambda}$ on the solid element, and then distribute it to the fluid mesh by a Delta function

$$\boldsymbol{\lambda}_{\mathrm{f}} = \sum_{\text{all elements}} \delta_h(\mathbf{x}_{\mathrm{f}} - \mathbf{x}_{\mathrm{s}}) \int_{E_i} \boldsymbol{\lambda}\, \mathrm{d}E_i, \tag{19}$$

where $\mathbf{x}_{\mathrm{f}}$ and $\mathbf{x}_{\mathrm{s}}$ are the locations of the fluid and solid nodes, respectively, and $\boldsymbol{\lambda}_{\mathrm{f}}$ denotes the value of $\boldsymbol{\lambda}$ on the fluid grids. The Delta function is approximated by:

$$\delta_h(\mathbf{x}) = d_h(x) \cdot d_h(y), \tag{20}$$

and

$$d_h(r) = \begin{cases} \frac{1}{8h}\left(3 - 2\frac{|r|}{h} + \sqrt{1 + 4\frac{|r|}{h} - 4\left(\frac{|r|}{h}\right)^2}\right), & |r| < h, \\ \frac{1}{8h}\left(5 - 2\frac{|r|}{h} - \sqrt{-7 + 12\frac{|r|}{h} - 4\left(\frac{|r|}{h}\right)^2}\right), & h \leqslant |r| \leqslant 2h, \\ 0, & \text{otherwise.} \end{cases}$$

From the above descriptions, it is found that some accuracy will be lost because the proposed algorithm does not describe the interface as accurately as the boundary-fitted algorithm does when the interface is not aligned with the fluid mesh. But the loss can be compensated by increasing the local mesh resolution. The multi-block method [25] or the meshless method [26] may be worth considering.

Because the full coupling scheme for the fluid–solid system requires large computational resources, we decouple the whole system to the fluid and solid sub-problems with the fractional step scheme in the same manner as in the DLM/FD [15,16,19]. The present fractional step scheme is the following:

(1) Assuming that f_i^n, $\boldsymbol{\lambda}^n$ at the time step n is given, calculate f_i^* from Eq. (1) without the collision operator and then ρ_{f}^* and $\mathbf{u}_{\mathrm{f}}^*$ from Eq. (2). Here, the superscript "*" denotes an intermediate fractional step.
(2) Based on Eqs. (11) and (17), find the solid displacement $\mathbf{d}_{\mathrm{s}}^{n+1}$ with the finite element method.
(3) Using the first-order accurate scheme, calculate the solid velocity from $\mathbf{u}_{\mathrm{s}}^{n+1} = \frac{\mathbf{d}_{\mathrm{s}}^{n+1} - \mathbf{d}_{\mathrm{s}}^{n}}{\delta_t}$. Together with the velocity constraint over the solid domain and the idea of the fractional time scheme, compute $\boldsymbol{\lambda}^{n+1}$ from the following equation:

$$\int_{\Omega_{\mathrm{s}}} \boldsymbol{\lambda}^{n+1} \cdot \boldsymbol{\varphi}_{\mathrm{s}} \, \mathrm{d}\Omega_{\mathrm{s}} = \int_{\Omega_{\mathrm{s}}} \boldsymbol{\lambda}^{n} \cdot \boldsymbol{\varphi}_{\mathrm{s}} \, \mathrm{d}\Omega_{\mathrm{s}} + \int_{\Omega_{\mathrm{s}}} \rho_{\mathrm{f}}^* \left(\frac{\mathbf{u}_{\mathrm{s}}^{n+1} - \mathbf{u}_{\mathrm{f}}^*}{\delta_t} \right) \cdot \boldsymbol{\varphi}_{\mathrm{s}} \, \mathrm{d}\Omega_{\mathrm{s}}. \tag{21}$$

(4) Calculate the intermediate distribution function f_i^{**} from:

$$f_i^{**} = f_i^* + \frac{w_i \delta_t}{c_{\mathrm{s}}^2} \left[\left(\boldsymbol{\lambda}_{\mathrm{f}}^{n+1} - \boldsymbol{\lambda}_{\mathrm{f}}^{n} \right) \cdot \mathbf{e}_i \right]. \tag{22}$$

(5) Calculate the distribution function f_i^{n+1} at the time step $n + 1$ from:

$$f_i^{n+1} = f_i^{**} - \frac{1}{\tau} (f_i^{**} - f_i^{\mathrm{eq}**}). \tag{23}$$

3. Numerical examples

3.1. Flow past a circular cylinder

This example is used to verify the algorithm, with emphasis on checking if the Lagrange multiplier is correctly imposed. The cylinder is assumed to be rigid and fixed in a uniform flow.

The drag coefficient is defined as:

$$C_{\mathrm{d}} = \frac{F_{\mathrm{c}x}}{0.5 \rho_{\mathrm{f}} U_\infty^2 D}, \tag{24}$$

and the lift coefficient is defined as:

$$C_{\mathrm{l}} = \frac{F_{\mathrm{c}y}}{0.5 \rho_{\mathrm{f}} U_\infty^2 D}, \tag{25}$$

where $F_{\mathrm{c}x}$ and $F_{\mathrm{c}y}$ are the streamwise and transverse components of the force on the cylinder with the diameter D, respectively. From the definition of the distributed Lagrange multiplier, for the current numerical example, we can calculate the force on the cylinder $\mathbf{F}_{\mathrm{c}}$ using:

$$\mathbf{F}_{\mathrm{c}} = -\int_{\Omega_{\mathrm{s}}} \boldsymbol{\lambda} \, \mathrm{d}\Omega_{\mathrm{s}}, \tag{26}$$

rather than determining the derivatives of the fluid stress on the cylinder boundary.

Three cases of the Reynolds numbers being 20, 40 and 100 are considered here. The computational conditions are: $\rho_{\mathrm{f}} = 1.0$, $D = 40\delta_x$, $\delta_x = \delta_t = 1$. The size of the rectangular fluid domain is $1100\delta_x \times 800\delta_x$, and the velocities on the top, bottom and inlet boundaries are given as $U_\infty = 0.1$. The cylinder is divided into 387 elements, as shown in Fig. 1. At the beginning, we set $\boldsymbol{\lambda} = 0$ and $\mathbf{u}_{\mathrm{f}} = 0$.

In the cases of $Re = 20$ and 40, the flow finally reaches a steady state and a symmetric wake region is formed at the rear of the cylinder, as illustrated in Fig. 3. The circulation region expands as the Reynolds

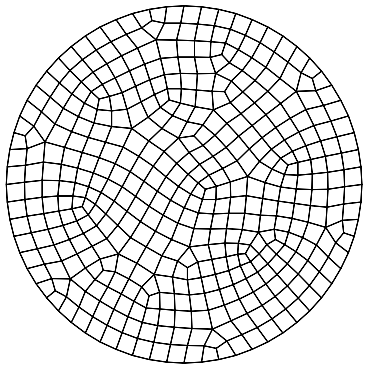

Fig. 1. The multiplier mesh.

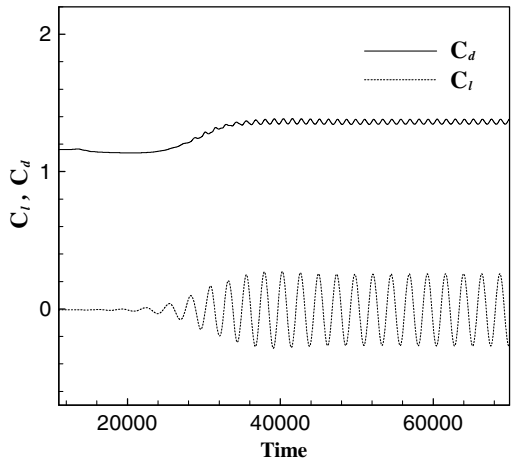

Fig. 2. The drag and lift coefficients at $Re = 100$.

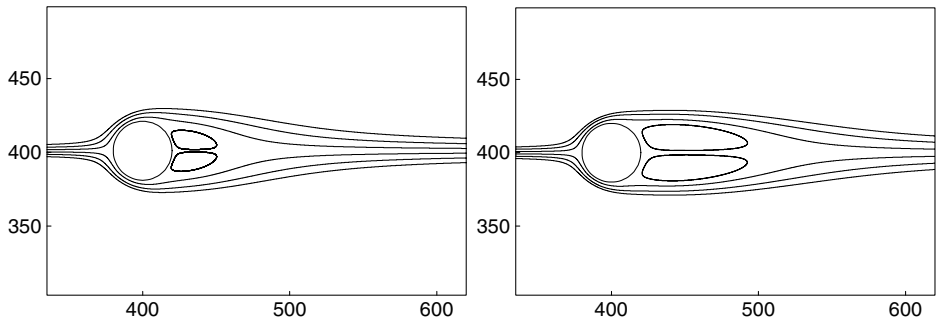

streamlines at Re=20 streamlines at Re=40

Fig. 3. Steady streamlines.

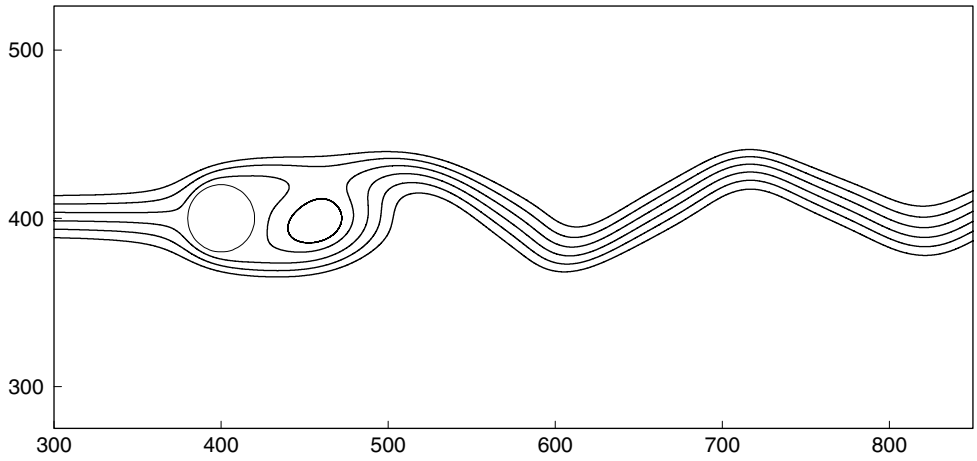

Fig. 4. Streamlines at Re = 100.

number increases. In order to compare our computation to the previous works, we define the non-dimensional recirculation length by $L^* = L_r/D$.

As the Reynolds number exceeds the critical value of 49, the flow becomes unsteady. Vortices are shed alternatively behind the cylinder and the Kármán vortex street is formed. The flow pattern at $Re = 100$ is depicted in Fig. 4. The corresponding time evolutions of the lift coefficient and drag coefficients (Fig. 2) reveal that the flow reaches a stable oscillatory status eventually. The oscillation frequency becomes an equally important quantity as the lift and drag coefficients. The dimensionless frequency is the so-called Strouhal number defined as:

$$St = \frac{f_v D}{U_\infty}, \tag{27}$$

where f_v is the dimensional frequency.

The quantitative comparisons are summarized in Table 1, and we can see that our results on the drag and lift coefficients, the wake length and the Strouhal number compare favorably with the previous results, indicating that the flow problem in the DLM/FD method can be solved with the LBM and the Lagrange multiplier can be replaced by an external force in the framework of the LBM. The proposed method provides an alternative choice for the implementation of the wall boundary condition in the LBM.

3.2. Flapping of a slender elastic body in the wake of a cylinder

To demonstrate the versatility of the proposed algorithm, we simulate the flapping of a slender beam in the wake of a cylinder. The flow schematic is shown in Fig. 5. The size of the beam is $100\delta_x \times 1.25\delta_x$. The distance between the fixed tip and the center of the cylinder, L, is 3D, and the distance between the fixed tip and the centerline of the flow field, h, is $0.5\delta_x$. The size of the fluid domain is $900\delta_x \times 320\delta_x$, and the size of the cylinder and the boundary conditions are the same as the above numerical example. The material parameters are given as: $C_1 = 3$, $K = 2 \times 10^5$. The Reynolds number based on the cylinder diameter is 133. The Lagrange multipliers on the cylinder and the beam are set to be zero initially. We define half the vertical distance between the centers of a pair of shed vortices as H, and we only give a rough estimate of H, because its value varies as the vortices move downstream.

Table 1
Comparison with previous studies

	$Re = 20$		$Re = 40$		$Re = 100$		
	C_d	L^*	C_d	L^*	C_d (mean)	ΔC_l	St
Tuann and Olson [27]	2.25	0.9	1.675	2.1	–	–	–
Fornberg [28]	2.000	0.91	1.498	2.24	–	–	–
He and Doolen [30]	2.152	0.921	1.499	2.245	–	–	–
Niu et al. [33]	2.111	0.96	1.574	2.265			
Saiki and Biringen [31]	–	–	–	–	1.26	–	0.171
Lai and Peskin [24]	–	–	–	–	1.4473	0.6598	0.165
Gresho et al. [29]	–	–	–	–	1.76	–	0.18
Chew et al. [34]					1.3668	0.75	0.164
Ding et al. [32]	2.18	0.93	1.713	2.20	1.325	0.56	0.164
Present	2.11	0.86	1.58	2.16	1.36	0.52	0.169

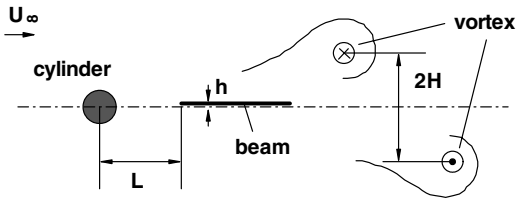

Fig. 5. Schematic of the flow.

Fig. 9 shows a sequence of vorticity contours during one period of the flapping. The time of each snapshot is shown in Fig. 6. Fig. 8 gives the vorticity contour without the beam near the time corresponding to "a" in Fig. 6.

As shown in Fig. 9, the beam swings with the oscillating wake and the vortex structure is modified by the beam. We find that the beam (except the front part) coincides with the interface between the negative and positive vorticity regions. The shape of the interface is flatter than the one without the beam in the flow field, which is ascribed to the dramatic swing of the end part of the beam.

Because the length of the beam is comparable to the wavelength of the Kármán vortex street, the presence of the beam significantly modifies the local cylinder wake structure at the region where the beam is

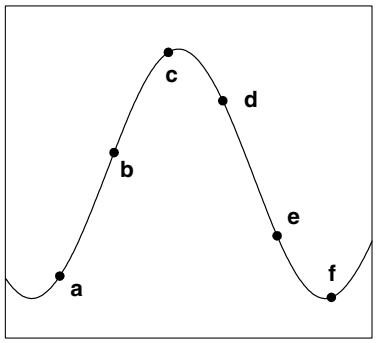

Fig. 6. Time sequences.

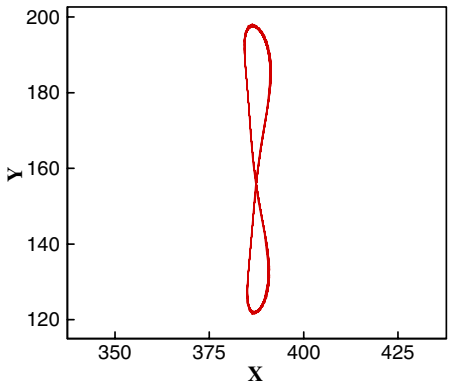

Fig. 7. Trajectory of the free tip.

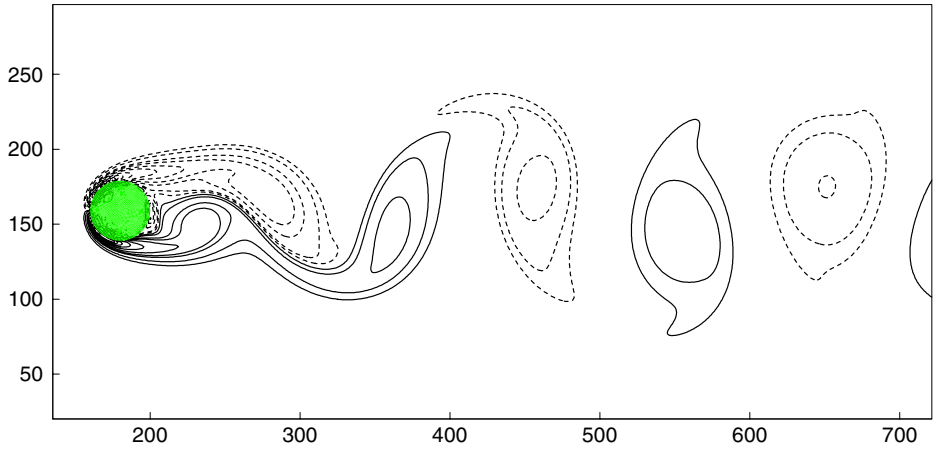

Fig. 8. Vorticity contour at $Re = 133$.

Table 2
Comparison of the parameters

	C_d (mean)	ΔC_l	St (cylinder)	St (beam)	H/D
Single cylinder	1.503	0.888	0.196	–	0.38
With beam	1.478	1.056	0.187	0.187	2.53

located (Fig. 9). With the flapping of the beam, the vortices are shed from the free tip, and the new type of Kármán vortex street is formed. From Figs. 8 and 9 and Table 2, H becomes larger when the beam is introduced to the wake. Fig. 7 illustrates the trajectory of the free tip, and we see that the oscillation amplitude of the beam free tip is larger than the diameter of the cylinder, which means that the beam throws the vortices farther away from the center line.

It is interesting that the trajectory of the beam free tip is '8'-shaped, as shown Fig. 7. Zhang et al. [35] investigated the flapping of a flexible filament in a soap film. Although the elastic body was not in the

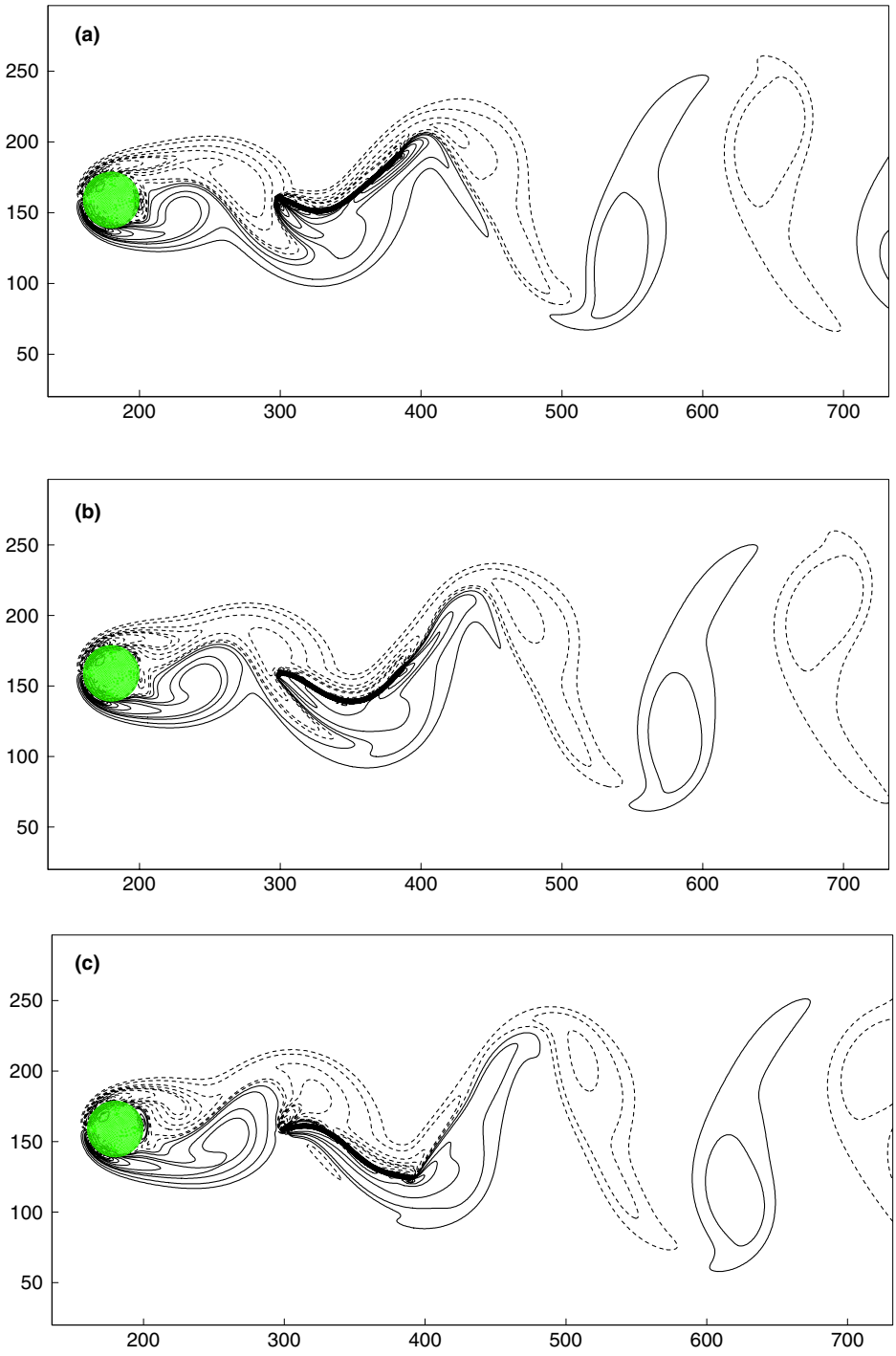

Fig. 9. The snapshots of the vorticity contours at different time (the solid lines denote the positive values and the dash lines denote the negative values).

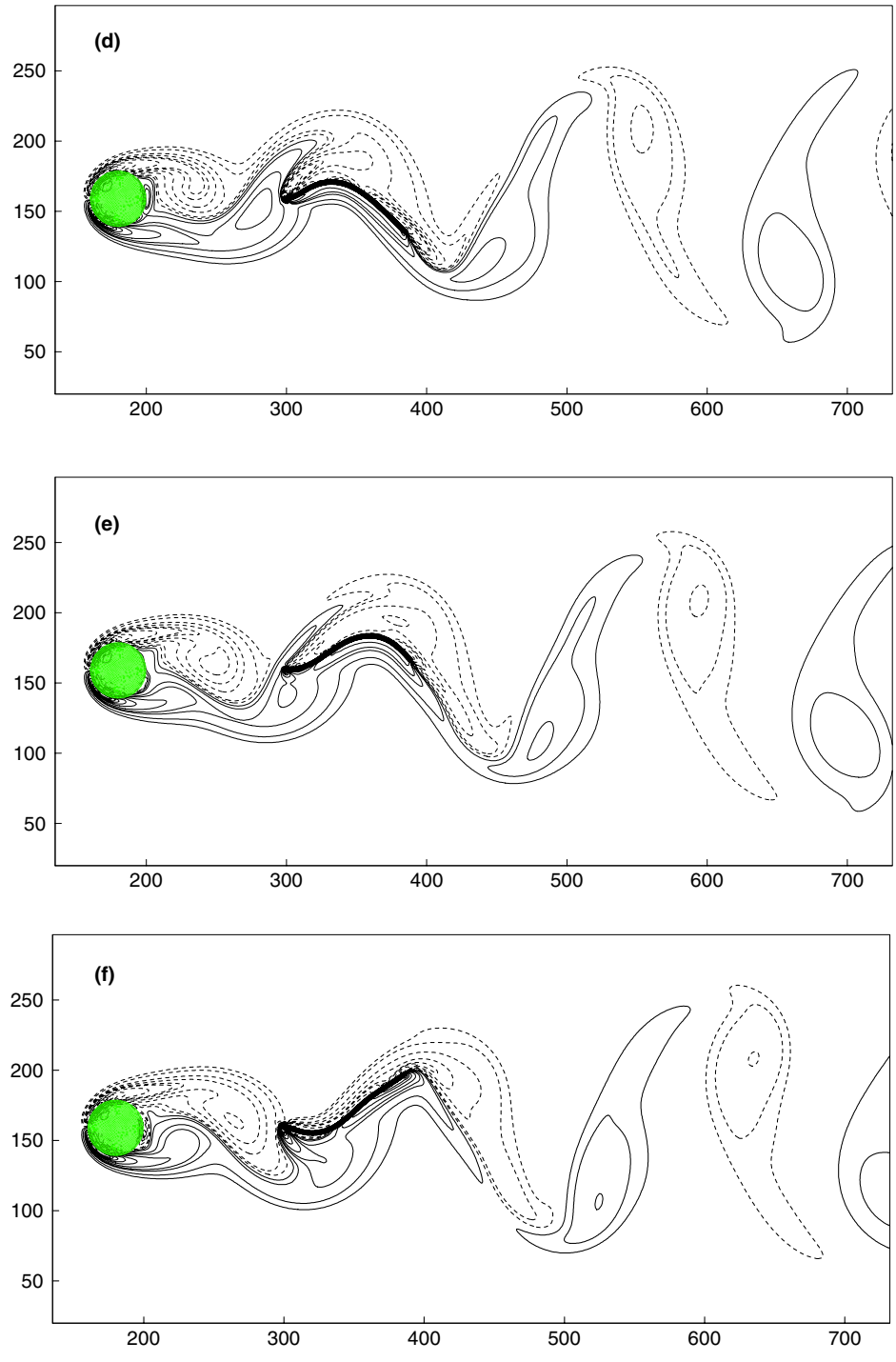

Fig. 9 (*continued*)

cylinder wake in their experiment, it flapped in the same fashion as observed in our simulations. However, Fig. 7 shows that the free tip trajectory is not symmetric and this indicates that the flapping motion is sensitive to the beam's location in the flow field. Although the fixed tip of the beam is only slightly deviated from the centerline ($0.5\delta_x$, i.e., 1/80 of the cylinder diameter), a significant asymmetry is observed.

The comparison of the lift coefficients, the drag coefficients and the Strouhal numbers between the two cases with and without the beam is concluded in Table 2. The data illustrate that the beam in the wake reduces the drag on the cylinder and that the flapping of the beam amplifies the fluctuation in the lift coefficient. The presence of the flexible beam also reduces the value of the Strouhal number, and it is observed that the beam flaps at the same frequency as the vortex shedding. The results reveal that there are interactions between the cylinder wake and the flapping of the beam, but the former plays a dominating role.

4. Conclusion

A new method for the fluid–structure interactions has been proposed. This method combines the ideas of the lattice Boltzmann method and the DLM/FD method, and has the following features:

1. The advantages of the lattice Boltzmann method are preserved. The lattice Boltzmann method has several distinguished features or advantages, such as the simple evolution equation and the linear convection operator, easy parallelization of the code, direct access to the pressure of the incompressible flow, and so on [1]. In our algorithm, we only modify the external force term, which does not compromise the advantages of the LBM.
2. The advantages of the fictitious domain method are inherited by the new method, making it convenient to deal with the complex boundary and the elastic deformation in fluid–structure interaction problems.

Two numerical examples have been utilized to verify the algorithm and illustrated the power of the method to deal with fluid/elastic–structure interactions. Although the fluid/rigid–structure interaction is not involved here, there is no particular difficulty in extending the algorithm to that area. Moreover, our algorithm provides an alternative boundary treatment in the lattice Boltzmann method.

Acknowledgment

We wish to thank Dr. Zhaosheng Yu for helpful discussions and suggestions on the distributed-Lagrange-multiplier/fictitious-domain method.

References

[1] S. Chen, G.D. Doolen, Lattice Boltzmann method for fluid flows, Annu. Rev. Fluid Mech. 30 (1998) 329.
[2] R.R. Nourgaliev, T.N. Dinh, T.G. Theofanous, D. Joseph, The lattice Boltzmann equation method: theoretical interpretation, numerics and implications, Int. J. Multiphase Flow 29 (2003) 117.
[3] X. Nie, G.D. Doolen, S.Y. Chen, Lattice Boltzmann simulation of fluid flows in MEMS, J. Stat. Phys. 107 (2002) 279.
[4] A.J. Wagner, L. Giraud, C.E. Scott, Simulation of a cusped bubble rising in a viscoelastic fluid with a new numerical method, Comput. Phys. Commun. 129 (2000) 227.
[5] I. Ispolatov, M. Grant, Lattice Boltzmann method for viscoelastic fluids, Phys. Rev. E 65 (2002) 65704.
[6] M. Krafczyk, J. Tölke, E. Rank, M. Schulz, Two-dimensional simulation of fluid–structure interaction using lattice-Boltzmann methods, Comput. Struct. 79 (2001) 2031.
[7] D. Qi, C.K. Aidun, A new method for analysis of the fluid interaction with a deformable membrane, J. Stat. Phys. 90 (1998) 145.

[8] A.J.C. Ladd, Numerical simulation of particulate suspensions via a discretized Boltzmann equation, Part 1. Theoretical foundation, J. Fluid Mech. 271 (1994) 285.
[9] A.J.C. Ladd, R. Verberg, Lattice-Boltzmann simulations of particle–fluid suspensions, J. Stat. Phys. 104 (2001) 1191.
[10] Z.-G. Feng, E.E. Michaelides, The immersed boundary-lattice Boltzmann method for solving fluid–particles interaction problems, J. Comput. Phys. 195 (2004) 602.
[11] C.S. Peskin, Numerical analysis of blood flow in the heart, J. Comput. Phys. 25 (1977) 220.
[12] J. Donea, S. Giuliani, J.P. Halleux, An arbitrary Lagrangian–Eulerian finite element method for transient dynamic fluid–structure interactions, Comput. Meth. Appl. Mech. Eng. 33 (1982) 689.
[13] R. Glowinski, T. Pan, J. Périaux, A fictitious domain method for Dirichlet problems and applications, Comput. Meth. Appl. Mech. Eng. 111 (1994) 283.
[14] R. Glowinski, T. Pan, J. Périaux, A fictitious domain method for external incompressible viscous flow modeled by Navier–Stokes equations, Comput. Meth. Appl. Mech. Eng. 112 (1994) 133.
[15] R. Glowinski, T. Pan, T.I. Hesla, D.D. Joseph, A distributed Lagrange multiplier/fictitious domain method for particulate flows, Int. J. Multiphase Flow 25 (1999) 755.
[16] Z. Yu, N. Phan-Thien, Y. Fan, R.I. Tanner, Viscoelastic mobility problem of a system of particles, J. Non-Newtonian Fluid Mech. 104 (2002) 87.
[17] F.P.T. Baaijens, A fictitious domain/mortar element method for fluid–structure interaction, Int. J. Numer. Meth. Fluids 35 (2001) 743.
[18] J. de Hart, G.W.M. Peters, P.J.G. Schreurs, F.P.T. Baaijens, A three-dimensional computational analysis of fluid–structure interaction in the aortic valve, J. Biomech. 36 (2003) 103.
[19] Z. Yu, A DLM/FD method for fluid/flexible–body interactions, J. Comput. Phys. (submitted).
[20] T. Lee, C. Lin, Pressure evolution lattice-Boltzmann-equation method for two-phase flow with phase change, Phys. Rev. E 67 (2003) 056703.
[21] Y. Qian, D. d'Humières, P. Lallemand, Lattice BGK models for Navier–Stokes equation, Europhys. Lett. 17 (1992) 479.
[22] T. Sussman, K.J. Bathe, A finite element formulation for nonlinear incompressible elastic and inelastic analysis, Comput. Struct. 26 (1987) 357.
[23] O.C. Zienkiewicz, K. Morgan, Finite Elements and Approximation, Wiley, Chichester, 1983.
[24] M.C. Lai, C.S. Peskin, An immersed boundary method with formal second order accuracy and reduced numerical viscosity, J. Comput. Phys. 160 (2000) 705.
[25] D. Yu, R. Mei, W. Shyy, A multi-block lattice Boltzmann method for viscous fluid flows, Int. J. Numer. Meth. Fluids 39 (2002) 99.
[26] C. Shu, Y.T. Chew, X.D. Niu, Least-squares-based lattice Boltzmann method: a meshless approach for simulation of flows with complex geometry, Phys. Rev. E 64 (2001) 045701.
[27] S.Y. Tuann, M.D. Olson, Numerical studies of the flow around a circular cylinder by a finite element method, Comput. Fluids 6 (1978) 219.
[28] B. Fornberg, A numerical study of steady viscous flow past a circular cylinder, J. Fluid Mech. 98 (1980) 819.
[29] P.M. Gresho, R. Chan, C. Upson, R. Lee, A modified finite element method for solving the time-dependent, incompressible Navier–Stokes equations: Part 2: applications, Int. J. Numer. Methods Fluids 4 (1984) 619.
[30] X. He, G. Doolen, Lattice Boltzmann method on curvilinear coordinates system: flow around a circular cylinder, J. Comput. Phys. 134 (1997) 306.
[31] E.M. Saiki, S. Biringen, Numerical simulation of a cylinder in uniform flow: application of a virtual boundary method, J. Comput. Phys. 123 (1996) 450.
[32] H. Ding, C. Shu, K.S. Yeo, D. Xu, Simulation of incompressible viscous flows past a circular cylinder by hybrid FD scheme and meshless least square-based finite difference method, Comput. Methods Appl. Mech. Eng. 193 (2004) 727.
[33] X.D. Niu, Y.T. Chew, C. Shu, Simulation of flows around an impulsively started circular cylinder by Taylor series expansion- and least squares-based lattice Boltzmann method, J. Comput. Phys. 188 (2003) 176.
[34] Y.T. Chew, C. Shu, X.D. Niu, Simulation of unsteady incompressible flows by using Taylor series expansion- and least square-based lattice Boltzmann method, Int. J. Mod. Phys. C 13 (2002) 719.
[35] J. Zhang, S. Childress, A. Libchaber, M. Shelley, Flexible filaments in a flowing soap film as a model for one-dimensional flags in a two-dimensional wind, Nature 408 (2000) 835.